Bioactive Materials 8 (2022) 341–354

Contents lists available at ScienceDirect

Bioactive Materials

journal homepage: www.sciencedirect.com/journal/bioactive-materials

Mussel-inspired adhesive antioxidant antibacterial hemostatic composite hydrogel wound dressing via photo-polymerization for infected skin wound healing

Yutong Yang [a,b], Yongping Liang [b], Jueying Chen [b], Xianglong Duan [a,c,**], Baolin Guo [b,*]

[a] Second Department of General Surgery, Shaanxi Provincial People's Hospital, Xi'an, 710068, China
[b] Frontier Institute of Science and Technology, and State Key Laboratory for Mechanical Behavior of Materials, and Key Laboratory of Shaanxi Province for Craniofacial Precision Medicine Research, College of Stomatology, Xi'an Jiaotong University, Xi'an, 710049, China
[c] Second Department of General Surgery, Third Affiliated Hospital of Xi'an Jiaotong University, Xi'an, 710068, China

ARTICLE INFO

Keywords:
Chitosan
Wound dressing
Antibacterial
Wound healing
Hemostat
Infected skin wound

ABSTRACT

With the increasing prevalence of drug-resistant bacterial infections and the slow healing of chronically infected wounds, the development of new antibacterial and accelerated wound healing dressings has become a serious challenge. In order to solve this problem, we developed photo-crosslinked multifunctional antibacterial adhesive anti-oxidant hemostatic hydrogel dressings based on polyethylene glycol monomethyl ether modified glycidyl methacrylate functionalized chitosan (CSG-PEG), methacrylamide dopamine (DMA) and zinc ion for disinfection of drug-resistant bacteria and promoting wound healing. The mechanical properties, rheological properties and morphology of hydrogels were characterized, and the biocompatibility of these hydrogels was studied through cell compatibility and blood compatibility tests. These hydrogels were tested for the in vitro blood-clotting ability of whole blood and showed good hemostatic ability in the mouse liver hemorrhage model and the mouse-tail amputation model. In addition, it has been confirmed that the multifunctional hydrogels have good inherent antibacterial properties against Methicillin-resistant *Staphylococcus aureus* (MRSA). In the full-thickness skin defect model infected with MRSA, the wound closure ratio, thickness of granulation tissue, number of collagen deposition, regeneration of blood vessels and hair follicles were measured. The inflammation-related cytokines (CD68) and angiogenesis-related cytokines (CD31) expressed during skin regeneration were studied. All results indicate that these multifunctional antibacterial adhesive hemostatic hydrogels have better healing effects than commercially available Tegaderm™ Film, revealing that they have become promising alternative in the healing of infected wounds.

1. Introduction

Skin constitute the largest multi-layered organ of the human body, which includes the epidermis and dermis [1,2], and it also acts as a barrier for body protection, such as preventing excessive evaporation of water, and protecting the human body from the invasion of pathogens [3–5]. However, once the entire epidermis severely injured, the skin will lose the most basic protective effect, especially the microbial infection of the wound site will severely prolong the healing process [6,7]. If it cannot be treated effectively in time, chronic wounds are easily colonized by pathogens such as *Escherichia coli*, *Staphylococcus aureus*, and *Staphylococcus epidermidis*, finally causing non-functional scar [8–10]. For a long time in the past, antibiotics have been widely and massively used, which inevitably leads to the emergence of drug-resistance [11–13]. Therefore, it is very important to develop antibiotic-free multifunctional wound dressings to treat bacterial infections.

Hydrogel has a unique three-dimensional network structure, composed of natural or synthetic polymers, and shows good water absorption and biodegradability [14,15]. In particular, hydrogels can provide a moist environment for callus and epithelial cells, and accelerate the deposition of collagen and the proliferation of fibroblasts [16–18], thereby effectively promoting epithelialization and speeding

Peer review under responsibility of KeAi Communications Co., Ltd.
* Corresponding author.
** Corresponding author. Second Department of General Surgery, Shaanxi Provincial People's Hospital, Xi'an, 710068, China.
E-mail addresses: duanxianglong@nwpu.edu.cn (X. Duan), baoling@mail.xjtu.edu.cn (B. Guo).

https://doi.org/10.1016/j.bioactmat.2021.06.014
Received 22 February 2021; Received in revised form 4 June 2021; Accepted 11 June 2021
Available online 23 June 2021

up wound healing [19–21]. Chitosan (CS) is a natural cationic polysaccharide which has been widely used in the preparation of hydrogels [22]. However, the application of chitosan is limited by its poor water solubility [23]. In consideration of solving this critical problem, CS is modified by various water-soluble groups. Polyethylene glycol monomethyl ether (mPEG) is a highly hydrophilic polymer, which is widely used in biomedical applications due to its excellent biocompatibility [24]. The modification of chitosan with mPEG (CS-PEG) not only improves the water solubility, increases the mechanical strength of the hydrogel, but also shows excellent biocompatibility [25,26]. In addition, study has shown that polysaccharides grafted with mPEG can promote hemostasis [27], which further expands the clinical use of mPEG grafted chitosan-based hydrogels. However, the antibacterial properties of CS-PEG are not enough to deal with wound healing caused by drug-resistant bacteria.

Among many antibacterial agent, antibacterial activity of metal ion is mild and efficient [28], which can not only effectively sterilize, but also avoid burns that may be caused by photo-thermal antibacterial methods [29]. Zinc ions can cause bacterial death, because zinc ions play an important role in inhibiting active transport and amino acid metabolism and enzyme system destruction [30]. In addition, electrostatic force from positively charged zinc ions and the negatively charged bacteria surface destroys the bacterial cell membrane, causing leakage of cell contents [17]. Furthermore, zinc ions can increase self-cleaning and keratinocyte migration during wound healing, which is useful during skin regeneration [31]. Metal nanoparticles are usually used as carriers for ion release [32]. However, metal nanoparticles are usually simply mixed in the hydrogel, which inevitably causes poor dispersibility [33]. In addition, metal particles degrade slowly and are not suitable for wound repair [32,34,35]. The coordination of zinc ions with the polymers might be a promising alternative approach. Zinc ions can form complexation with hydroxyl group and amine groups. As an important adhesive and antioxidant, dopamine with hydroxyl groups can form a stable complexation effect with zinc ions [36,37]. Furthermore, hydrogels containing dopamine usually show excellent tissue adhesion mainly due to the interaction between catechol groups and amino or thiol group of the tissues [38], and they exhibited good adhesion with the tissue to achieve hemostasis [39]. In addition, the antioxidant capacity of dopamine can effectively relieve the oxidative stress of the wound site and improve the speed of wound repair [40]. However, the complexion of zinc ions with dopamine has not been reported for wound dressing.

Among the various gel polymerization methods, photo-initiated polymerization can control the formation of hydrogel in space and time [41], and has better polymerization efficiency and is unaffected by temperature conditions [42]. Photo-polymerization has been widely used to prepare biomaterials for drug delivery and tissue engineering. However, there are few reports on photo-crosslinked hydrogels for wound repair.

In this work, we developed adhesive antioxidant antibacterial hemostatic composite hydrogels based on polyethylene glycol monomethyl ether modified glycidyl methacrylate functionalized chitosan (CSG-PEG) and double bond modified-dopamine (DMA) and zinc ions via photo-polymerization and the coordination of zinc ions with the catechol group of dopamine. The rheological properties, mechanical properties, and adhesion properties of the obtained hydrogels were characterized. In addition, the inherent antibacterial ability, blood-clotting ability, and hemostasis ability of these hydrogels were tested. Besides, the biocompatibility of CSG-PEG/DMA/Zn hydrogel is tested by blood compatibility and cell compatibility. Finally, in a mouse model of full-thickness skin defect infected by drug-resistant bacteria MRSA, the CSG-PEG/DMA/Zn hydrogel was explored to promote the regeneration of blood vessels and hair follicles and to further enhance wound healing. All the results indicated that these multifunctional antibacterial hydrogels have enhanced hemostasis and wound healing effects in infected skin tissue defects, showing great potential for clinical application.

2. Materials and method

2.1. Materials

Chitosan (M_n = 100 000–300 000 Da), dopamine hydrochloride (DA) (purity 98%) and succinic anhydride were obtained from J&K. Polyethylene glycol monomethyl ether (mPEG), methacrylate anhydride (94%), glycidyl methacrylate (≥97%) and zinc chloride were purchased from Sigma-Aldrich. All other reagents were used without further purification.

2.2. Synthesis of mPEG-COOH and CSG-PEG

mPEG-COOH was first synthesized by improving the previously reported method [43]. In short, the active carboxyl end of mPEG is prepared by using succinic anhydride. The specific process of synthesizing mPEG-COOH is shown in the supplementary information (SI).

CSG-PEG is prepared by a two-step one-pot approach based on the reaction between the carboxyl group of mPEG-COOH, the epoxy group on glycidyl methacrylate and the amino group on chitosan. The specific process is shown in SI.

2.3. Synthesis of DMA and LAP

Methacrylamide dopamine (DMA) and lithium acylphosphinate (LAP) were synthesized using the reported method [44]. The specific process is shown in SI.

2.4. Preparation of CSG-PEG/DMA/Zn hydrogel

First, CSG-PEG, DMA, zinc chloride, and LAP were dissolved with concentration of 25 wt%, 10 wt%, 4.5 wt%, and 1 wt% respectively. The molar ratio of zinc ions to DMA was set as 1:2, and the corresponding mixed solution of zinc chloride and DMA was prepared. The final concentrations of DMA3, DMA6, and DMA9 were 0.3 wt% (15 μL), 0.6 wt% (30 μL), and 0.9 wt% (45 μL), respectively. The zinc ions final concentration corresponding to DMA was 0.09 wt% (10 μL), 0.18 wt% (20 μL), and 0.27 wt% (30 μL), respectively. Next, 400 μL of CSG-PEG solution was uniformly mixed with a fixed ratio of DMA/Zn mixture solution (the molar ratio is 2:1), then the LAP aqueous solution with a final concentration of 0.05 wt% (25 μL) was added under stirring and make up the volume of the hydrogel precursor solution to 500 μL with DI water. Finally, hydrogel pre-polymer was put under the excitation of ultraviolet light (365 nm) for 15 s, and after a while, the sol-gel transition completed.

2.5. Characterizations

The nuclear magnetic resonance (^{1}H NMR), and Fourier transform infrared spectroscopy (FT-IR) were used to confirm the successful preparation of DMA, mPEG-COOH and CSG-PEG. The equilibrium swelling ratio, in vitro degradability, and scanning electron microscope (SEM) were used to confirm swelling and degradation properties and the morphology of CSG-PEG/DMA/Zn hydrogels. The specific processes are shown in SI.

2.6. Rheological and mechanical test of hydrogels

The modulus of these hydrogels is measured by using a TA rheometer (dhr-2), and the modulus changes over time are recorded [45]. Compressive stress-strain curve of CSG-PEG/DMA/Zn hydrogels was obtained by a cyclic compression test with modification according to our previous report [46]. The specific process is shown in SI.

2.7. Adhesion strength test and antioxidant efficiency of hydrogels

The adhesion property of the CSG-PEG/DMA/Zn hydrogels was evaluated by a lap-shear test based on the previous study [47]. The specific processes are shown in SI.

The antioxidant capacity of these hydrogels by scavenging the stable 1,1-diphenyl-2-pyridohydrazino (DPPH) free radicals was evaluated by referring to previous report [48]. The specific process is shown in SI.

2.8. In vitro whole blood-clotting performance

The in vitro whole blood-clotting test was performed according to the previous method [49]. The specific process is shown in SI.

2.9. Hemolytic test of hydrogels

A fixed amount of hydrogel was mixed with blood cells, incubated at 37 °C for 1 h, and then the absorbance at 540 nm was tested to evaluate hemolysis [50]. The specific processes are shown in SI.

2.10. Hemostasis performance of hydrogels

Referring to previous research, the hemostatic capability of the CSG-PEG/DMA/Zn hydrogel was tested by employing a mouse liver hemorrhage model, and mouse-tail amputation model (Kunming mice, 30–35 g, female). The specific process is shown in SI.

2.11. Antibacterial property and zinc ions release test of hydrogels

The antibacterial ability of hydrogels was evaluated through contact antibacterial test and MIC test. 10 μL of bacterial suspension (10^6 CFU/mL) was mixed with the hydrogel in a 48-well plate, then 10 μL of bacterial suspension without materials was used as a control. After incubating the plate at 37 °C for 2 h, a certain amount of sterile PBS was added to each well to re-suspend the surviving bacteria. After incubating at 37 °C for 18–24 h, the colony forming unit (CFU) was calculated on the petri dish [51]. The specific processes are shown in SI. The detailed information of MIC test is shown in SI.

The zinc ion release performance of the hydrogels is tested by a zinc ions kit assay, and the details are shown in the SI.

2.12. Cytocompatibility test of hydrogels

The cytocompatibility test was performed by using leaching solution method and direct contact method according to previous research [52]. The specific process is shown in SI.

2.13. In vivo wound healing evaluation with a drug-resistant bacterial infected full-thickness skin defect model

To further evaluate the enhanced effect of CSG-PEG/DMA/Zn hydrogel on wound healing, a full-thickness skin defect model of MRSA infection was established. Hematoxylin-eosin (H&E) staining was used for histomorphological measurement at different stages of wound regeneration to assess inflammation and epidermal regeneration in the wound area. The collagen amount was evaluated by Masson trichrome staining and commercial kits (Jiancheng bioengineering, China) were used to estimate the content of hydroxyproline [4]. All operations followed the manufacturer's instructions. The specific process is shown in SI. All the animal experiments were approved by the institutional review board of Xi'an Jiaotong University.

2.14. Histology and immunohistochemistry

Histological and immunohistochemistry examinations were performed to assess the vascular remodeling and inflammatory cells during wound healing. CD31 and CD68 were selected for the immunohistochemistry staining [3]. The specific process is shown in SI.

2.15. Statistical analysis

Statistical analysis on all experimental data of the study was performed, and the results are expressed as mean ± standard deviation (SD). A one-way analysis of variance (ANOVA) followed by Bonferroni post-hoc test was used to make multiple comparisons with SPSS version 24 (IBM) to determine statistical differences ($P < 0.05$).

3. Results and discussion

3.1. Preparation of CSG-PEG/DMA/Zn hydrogel

Chronic wounds infected by MRSA have a high mortality ratio worldwide, so there is an urgent need to develop a series of new hydrogel dressings to address this issue. The regeneration of full-thickness skin wound is a complicated process, which needs many functions of the materials to fulfill this process, including antibacterial property to kill the bacteria, good hemostasis to stop bleeding, and antioxidant property to promote wound healing, ect. However, such multi-functional hydrogel wound dressing is rarely reported. In this study, a series of multifunctional antibacterial and antioxidant adhesion hemostatic hydrogels for wound healing of drug-resistant bacterial infections have been developed. CS is a natural cationic polysaccharide, which is widely used due to its excellent wound healing effect [53], hemostatic ability [54], and antibacterial activity [55]. However, the poor solubility of CS limits its further application [56]. Thus, a series of chitosan derivatives was designed to improve the solubility in water. For example, quaternized chitosan has been widely used, but highly quaternized modification can cause severe cytotoxicity [57]. In this work, as shown in Fig. 1a, mPEG-modified chitosan (CS-PEG) with good biocompatibility and improved solubility was developed by amidation reaction of polyethylene glycol monomethyl ether onto the backbone of CS in an aqueous solution. Furthermore, a double bond was introduced to CS-PEG by grafting glycidyl methacrylate to endow the polymer of CS-PEG with the ability that can form the basic network of the hydrogels by photo-initiated radical polymerization [41]. At the same time, double bond modified-dopamine (DMA) was synthesized in hopes of improving the adhesion and antioxidant capacity of the dressings. Besides, zinc ions was introduced to improve the antibacterial properties of hydrogels [51]. The hydrogel precursor premix was obtained by mixing the zinc chloride ($ZnCl_2$) aqueous solution with CSG-PEG and DMA. Subsequently, dual network cross-linked hydrogel was formed with LAP as photo-initiator through the polymerization of double bonds that derived from CSG-PEG and DMA. At the same time, zinc ions uniformly dispersed in the hydrogel network and coordinated with catechol group of dopamine. The covalent cross-linking between CSG-PEG and DMA serves as the main backbone component of the hydrogel network, and the stacking of dopamine benzene rings, the coordination of metal ions with catechol group and the hydrogen bonding give the hydrogel a second non-covalent physical crosslinking network (Fig. 1b). The mutual coordination of the dual networks contributes to the energy dissipation of the entire system, so that the hydrogel can withstand a certain degree of deformation imposed by external mechanical forces. Zinc ions were uniformly dispersed in the hydrogel system, not only as a cross-linking component, but also show the antibacterial properties [51]. At the same time, zinc ions can also promote the formation of epithelial tissue during wound healing [31]. By increasing the DMA concentration from 0 wt% to 0.3 wt%, 0.6 wt%, and 0.9 wt% (relative to the weight of the total hydrogel precursor) and setting the molar ratio of zinc ions concentration to DMA of 1:2, the zinc ions concentration corresponding to the DMA concentration is 0.09 wt%, 0.18 wt%, and 0.27 wt% respectively, a series of hydrogels with different rheology, morphology, and mechanical properties were obtained (Fig. 2a). The

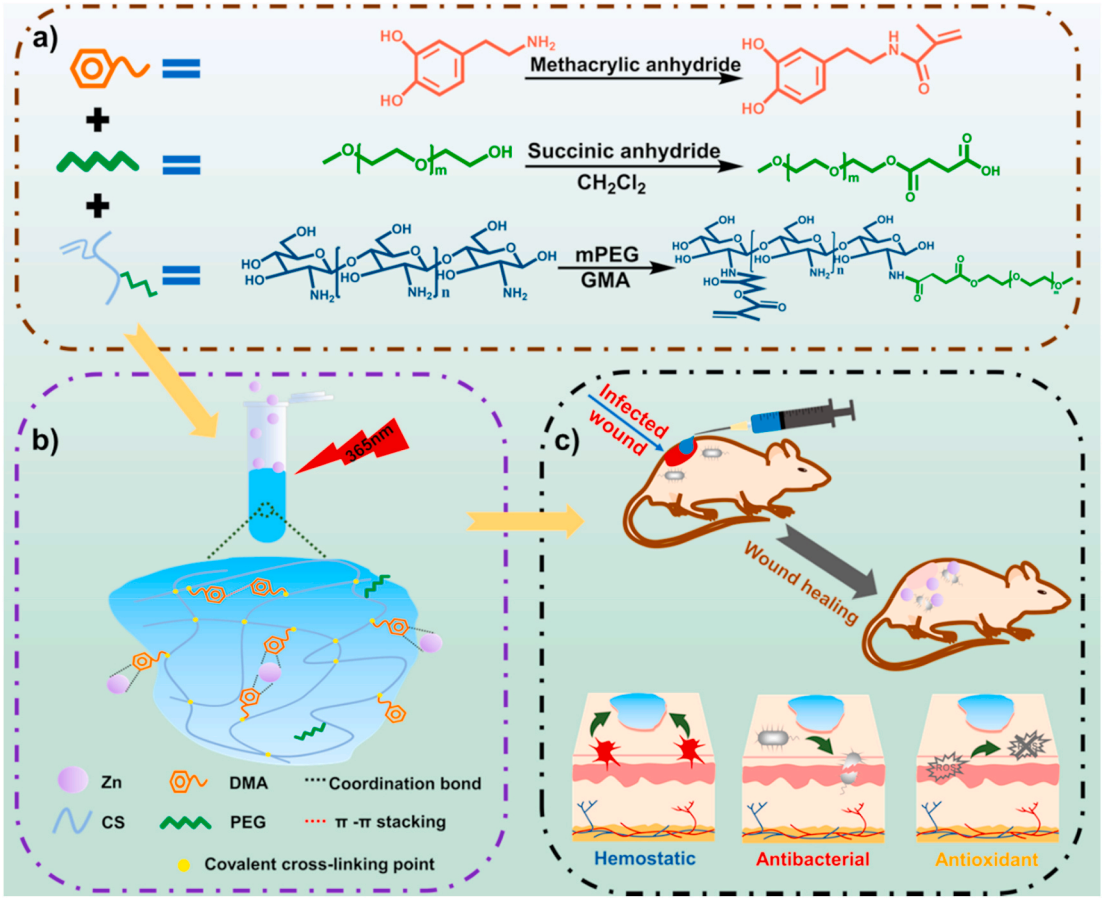

Fig. 1. (a) Synthesis of DMA, mPEG-COOH, and CSG-PEG; (b) Schematic representation of the CSG-PEG/DMA/Zn hydrogel formation; (c) Properties of hydrogel and its application in infected wound healing.

hydrogels were named as CSG-PEG, CSG-PEG/DMA3/Zn, CSG-PEG/DMA6/Zn, and CSG-PEG/DMA9/Zn as shown in Fig. S1. The obtained adhesive, antioxidant, antibacterial and hemostasis dual network hydrogels were used as a wound dressing during the repair of infected wounds (Fig. 1c).

The chemical structure of DMA, mPEG-COOH, CSG-PEG and CSG-PEG/DMA/Zn hydrogel was studied by FT-IR spectroscopy (Fig. 2b). For DMA, the characteristic signal at 1650 cm^{-1} was attributed to the stretching vibration of C═O in the amide group, indicating that amidation reaction occurred during the synthesis of DMA [58]. In addition, the characteristic signal around 3225 cm^{-1}exhibited the stretching vibration of –OH in catechol group. For mPEG-COOH, the absorption peaks of C═O and –COO with stretching and antisymmetric stretching vibration occurred at 1735 $cm^{-1}$and 1560 cm^{-1}, respectively, indicating that mPEG has been successfully carboxylated [59]. For CSG-PEG, the absorption peak related to mPEG appeared at 840 cm^{-1} and 960 cm^{-1}, and the absorption peak of double bond was about 1660 cm^{-1}, indicating that mPEG and glycidyl methacylate have been successfully grafted to CS [60]. The ^{1}H nuclear magnetic resonance (^{1}H NMR) analysis results of DMA, mPEG-COOH and CSG-PEG (Figs. S2–S4) further proved the successful modification of the dopamine, mPEG and CS. Compared with the infrared spectrum of CSG-PEG, the peak of CSG-PEG/DMA/Zn hydrogel at 1660 cm^{-1} disappeared, which indicated that DMA and CSG-PEG were polymerized via photo-polymerization of double bond.

3.2. Gelation time, swelling, degradation, rheology, and mechanical properties of hydrogels

The gelation time of hydrogel is very important in clinical and biomedical applications [61]. The gelation time of hydrogels was evaluated by the duration of UV light irradiation, and the gelation time of CSG-PEG, CSG-PEG/DMA3/Zn, CSG-PEG/DMA6/Zn, and CSG-PEG/DMA9/Zn hydrogels was about 15 s, and this dose of irradiation is safe for biological tissues [62] and is good for their in vivo application.

Tissue exudates are produced when the skin is wounded, and excessive exudate will cause bacteria to proliferate and affect the wound healing process. Hydrogel can absorb excess exudate from the wound while maintaining a moist environment [63]. Therefore, the swelling properties of these hydrogels were tested, and equilibrium swelling ratio (ESR) were used to evaluate the water swelling degree of different hydrogels under physiological conditions in vitro 37 °C PBS buffer (Fig. 2c). After all hydrogels reached swelling equilibrium, the ESR of CSG-PEG, CSG-PEG/DMA3/Zn, CSG-PEG/DMA6/Zn and CSG-PEG/DMA9/Zn were 1607% ± 125%, 1536% ± 71%, 1321% ± 90% and 1140% ± 91%, respectively. The results indicated that the hydrogel with higher DMA and zinc ions content showed lower ESR, which was attributed to the higher cross-linking density due to higher content of zinc ions and DMA, and the hydrophobic nature of DMA and the hydrophobic interaction between DMAs via π-π stacking are additional reasons that lead to lower ESR of the hydrogels containing the DMA.

The degradation behavior of these hydrogels in 37 °C PBS buffer (pH = 7.4) was evaluated by simulating the physiological environment in

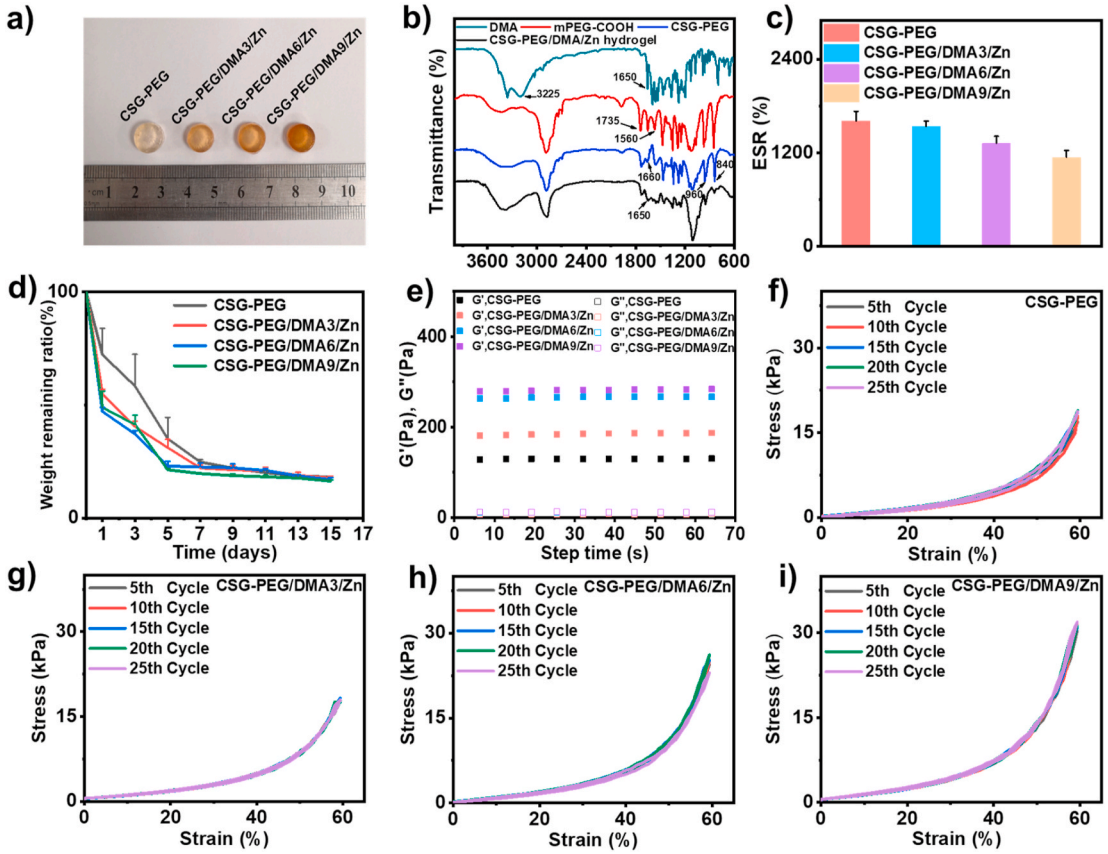

Fig. 2. Characterization of CSG-PEG/DMA/Zn hydrogels. (a) Photographs of different hydrogels; (b) FT-IR spectra of DMA, mPEG-COOH, CSG-PEG, and CSG-PEG/DMA/Zn hydrogel; (c) Equilibrium swelling ratio (ESR) of hydrogels (n = 3); (d) In vitro degradation curve of hydrogels (n = 3); (e) Rheological behavior of hydrogels; (f–i) Compressive stress-strain curve of CSG-PEG, CSG-PEG/DMA3/Zn, CSG-PEG/DMA6/Zn, and CSG-PEG/DMA9/Zn hydrogels at 60% strain.

vivo (Fig. 2d). After immersing the hydrogels in PBS for 3 days, the weight remaining ratio of CSG-PEG hydrogel was 60% of the initial weight, which might be because the unreacted CSG-PEG residuals in the network would diffuse out of the hydrogel matrix to cause the higher weight loss of the hydrogels in the first 3 days. While the weight remaining ratio of the CSG-PEG/DMA3/Zn, CSG-PEG/DMA6/Zn and CSG-PEG/DMA9/Zn hydrogels was 40% of the initial weight. After 13 days, the residual weight of all hydrogel groups remained at about 20%, demonstrating that CSG-PEG/DMA/Zn hydrogels showed tunable degradation rate.

The rheological properties of hydrogels were evaluated, and the temperature was set to 37 °C to simulate body temperature during the test [64]. The storage modulus (G′) and loss modulus (G″) of different hydrogels were tested at a fixed frequency (10 rad s^{-1}) (Fig. 2e). The minimum storage modulus of CSG-PEG hydrogel was approximately 130 Pa. With the increase of DMA and zinc ions, the storage modulus of CSG-PEG/DMA3/Zn and CSG-PEG/DMA6/Zn hydrogels increased to 185 Pa and 265 Pa. CSG-PEG/DMA9/Zn hydrogel showed the highest storage modulus of approximately 283 Pa. These results proved that with the increase of DMA and zinc ions, the non-covalent interaction becomes more obvious leading to the gradual increase of modulus of the hydrogel.

The good resilience of different hydrogels has been confirmed by cyclic compression test (Fig. 2f–i). When a fixed compressive strain of 60% was applied to the hydrogel, no obvious damage was seen to the hydrogel, indicating that the hydrogel can withstand a high degree of morphological compression. After 25 loading-unloading cycles, all hydrogel groups can still recover to their original shape in a short time, and the stress-strain curves almost completely overlapped, indicating that these hydrogels have good compressibility. With the increase in the ratio of DMA and zinc ions, the hydrogel had a higher compressive stress. The compressive stress of CSG-PEG/DMA3/Zn, CSG-PEG/DMA6/Zn, and CSG-PEG/DMA9/Zn hydrogels at strain of 60% were 19 kPa, 25 kPa, and 37 kPa, respectively, higher than that of CSG-PEG hydrogel (18 kPa). All these results indicated that CSG-PEG/DMA/Zn hydrogels have good energy dissipation capacity when external forces are applied because of the non-covalent cross-linking network.

3.3. Morphology, adhesion, and antioxidation of hydrogels

The uniform and interconnected morphology of these CSG-PEG/DMA/Zn hydrogels were observed with a scanning electron microscope (SEM) as shown in Fig. 3a. After hydrogels were freeze-dried, all the hydrogels showed similar pore size, and the range of pore size distribution is 50–170 μm. Specifically, as the content of DMA and zinc ions increased, the average pore size of CSG-PEG, CSG-PEG/DMA3/Zn, CSG-PEG/DMA6/Zn, and CSG-PEG/DMA9/Zn hydrogels decreased obviously, and they were 129.9 ± 19.1 μm, 111.1 ± 13.8 μm, 102.5 ± 14.3 μm, and 88.5 ± 11.5 μm, respectively (Fig. 3b). This may be due to the π-π interaction between DMA and the coordination interaction between catechol group of DMA and zinc ions increasing the degree of cross-linking of the hydrogel [65].

When hydrogel wound dressing is applied to wound area, the good tissue adhesion of hydrogel can promote to form a physical barrier to prevent bacterial invasion, and provide a moist environment to accelerate wound healing [66]. Thus, the adhesion strength of hydrogel was tested to evaluate the tissue adhesion in vitro by conducting a lap shear test with some modification (Fig. 3d) [47]. CSG-PEG hydrogel exhibited the lowest adhesion strength of 6.7 kPa, and the adhesion strength of the hydrogel increased from 7.3 kPa to 11.5 kPa (Fig. 3c) by increasing the

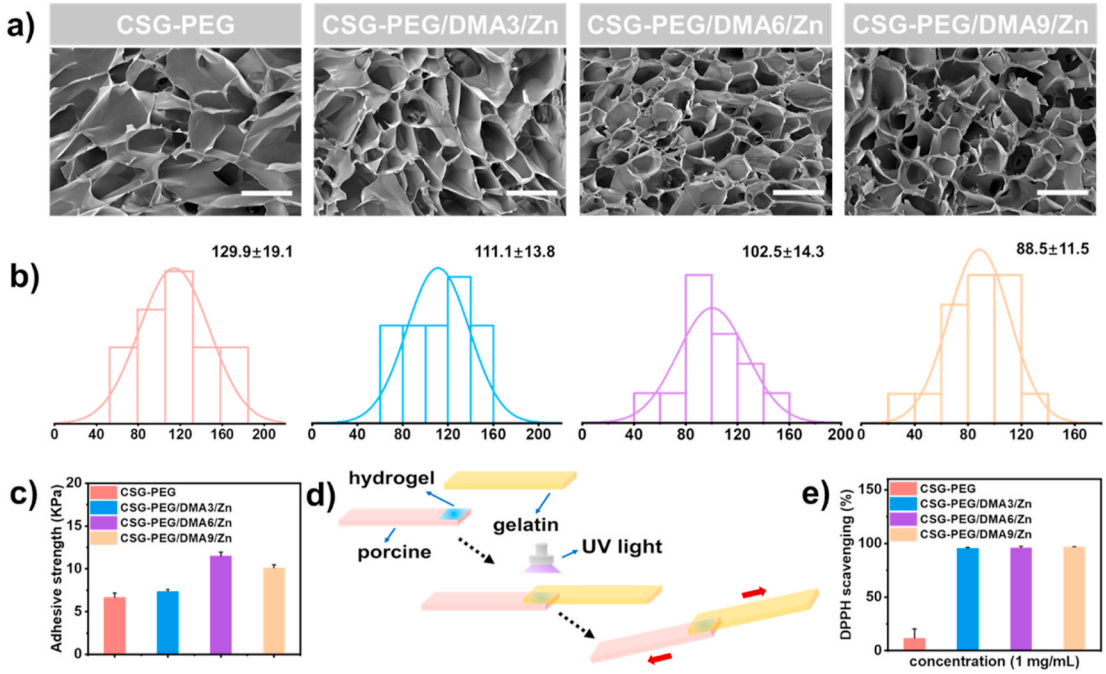

Fig. 3. Morphology, adhesion and antioxidation of CSG-PEG/DMA/Zn hydrogels. (a) SEM images of hydrogels, scale bar: 200 μm; (b) Pore size distribution of hydrogels; (c) Adhesion strength of hydrogels; d) Schematic presentation of the hydrogel adhesion test; e) DPPH scavenging percentage with a concentration of 1 mg/mL hydrogels after hydrogels contact with DPPH for 0.5 h.

content of DMA and zinc ions. However, the decrease in adhesion strength of CSG-PEG/DMA9/Zn hydrogel is mainly due to the increase in storage modulus of hydrogel [67]. The good adhesion property of the hydrogel was attributed to the following reasons. Firstly, the catechol groups and quinone groups on CSG-PEG/DMA/Zn hydrogel interact with the amino or thiol group of the tissues improving the adhesion strength of the dressings [25]. Besides, chitosan interacts with the phospholipid bilayer on the cell membrane through electrostatic and hydrophobic interactions which can also contribute to the adhesion strength [68]. In general, the adhesion strength of all hydrogel groups is better than commercial dressings (about 5 kPa) [69], and these hydrogels can effectively bond to the surface of the skin tissue as wound dressing.

A large number of free radicals can be produced at the wound site, which will lead to lipid peroxidation, DNA fragmentation and enzyme inactivation [68]. It has been proven that the use of materials containing free radical scavenging capabilities on the wound site can promote wound healing [10]. The free radical scavenging performance was evaluated by the DPPH free radical scavenging efficiency of the hydrogel with a dry weight of 1 mg/mL. As shown in Fig. 3e, the CSG-PEG hydrogel only showed a small amount of free radical scavenging efficiency, which may be because the CS has a certain degree of free radical scavenging capacity [70]. It is worth mentioning that the free radical scavenging efficiency of CSG-PEG/DMA3/Zn, CSG-PEG/DMA6/Zn, and CSG-PEG/DMA9/Zn hydrogels were all above 95%. The amount of DPPH scavenger contained in the dry weight of CSG-PEG/DMA6/Zn hydrogels of 1 mg/mL which was 131.6 μmol, and its amount is close to the molar amount of DPPH (100 μmol). So with respect to DPPH, the amount of DPPH scavenger was not much excessive. Overall, the good free radical scavenging ability of CSG-PEG/DMA/Zn hydrogel makes it have potential value for clinical wound healing applications.

3.4. In vitro whole blood-clotting test, blood compatibility, and in vivo hemostasis of hydrogels

When the skin is wounded, it will inevitably cause a certain degree of bleeding, so hemostasis is the first stage of wound healing [71]. An ideal wound dressing should promote platelets to aggregate at the wound site and form a blood clot to accelerate the hemostasis [49,72]. In vitro whole blood-clotting test is a common method to evaluate the blood clotting ability of hemostatic hydrogel [73], and a lower blood-clotting index (BCI) indicates a higher blood-clotting efficiency. Commercial gelatin sponge and gauze were selected as the control group of hemostatic agents. After incubating the different dressings with blood for 10 min at 37 °C, the results showed that BCI values of all hydrogel groups were lower than gauze and gelatin sponge ($P < 0.05$) (Fig. 4a). In addition, the BCI index of all hydrogel groups was lower than that of carboxymethyl cellulose cross-linked gelatin-PEG hydrogel reported by other researchers [74]. These results indicated that CSG-PEG/DMA/Zn hydrogels have more significant hemostatic ability compared to gauze and gelatin sponge.

Good blood compatibility is a prerequisite for the application of biomaterials [75,76]. The blood compatibility of CSG-PEG/DMA/Zn hydrogels were evaluated by in vitro hemolysis test. After incubating for 1 h in a simulated physiological environment in vitro, the appearance and color of four hydrogel groups and the positive control group (Triton X-100) were observed (Fig. 4b). All the hydrogel groups were slightly light yellow and consistent with PBS color, while the positive control group was bright red. Quantitative results showed the hemolysis ratio of all hydrogels was less than 5%. CSG-PEG showed the lowest hemolysis ratio of 1.97%. With the increase of the content of DMA and zinc ions, the hemolysis ratio of CSG-PEG/DMA3/Zn, CSG-PEG/DMA6/Zn, and CSG-PEG/DMA9/Zn hydrogels were 2.21%, 2.48%, and 2.79%, respectively, proving that these hydrogels have good blood compatibility.

Because the CSG-PEG/DMA6/Zn hydrogel exhibited the best adhesion strength, good blood compatibility and blood-clotting index, the hemostatic performance of CSG-PEG/DMA6/Zn was further evaluated in mouse liver hemorrhage model and mouse-tail amputation model (Fig. 4c–h). In the mouse liver hemorrhage model (Fig. 4c), compared with the blank group (689.2 ± 33.8 mg), the blood loss of CSG-PEG/DMA6/Zn hydrogel was significantly reduced (223.7 ± 13.8 mg) ($P < 0.01$) (Fig. 4g). Next, the hemostatic performance of the mouse-tail amputation model was tested (Fig. 4d), and the blood loss of CSG-

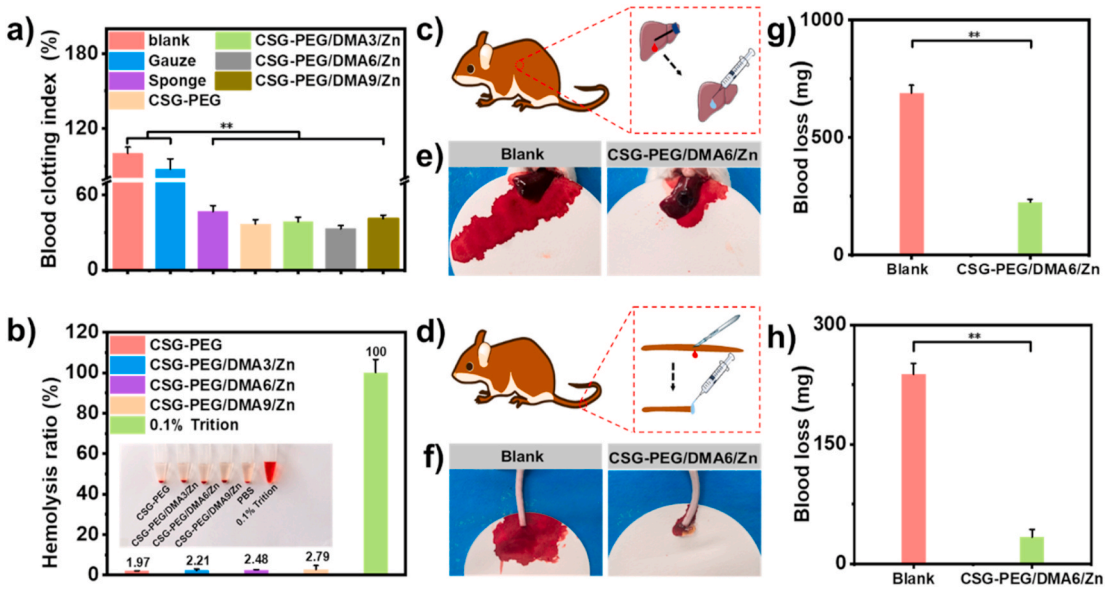

Fig. 4. Whole blood-clotting, blood compatibility, and in vivo hemostasis test of CSG-PEG/DMA/Zn hydrogels. (a) Dynamic whole blood-clotting test; (b) Hemolysis ratio (%) of hydrogels; Schematic representation of (c) mouse liver hemorrhage model and (d) mouse-tail amputation model; Bloodstain photographs of (e) mouse liver hemorrhage model and (f) mouse-tail amputation model; Quantitative results of blood loss (n = 4) of (g) mouse liver hemorrhage model and h) mouse-tail amputation model. *P < 0.05, **P < 0.01.

PEG/DMA6/Zn hydrogel was significantly reduced (33.4 ± 9.7 mg) compared with the blank group (237.8 ± 13.6 mg) (P < 0.01) (Fig. 4h), and it is worth mentioning that the blood loss of CSG-PEG/DMA6/Zn hydrogel is far less than the previously reported chitosan-based wound dressing (261.28 ± 35.61 mg) [77]. The hemostatic effect of CSG-PEG/DMA6/Zn hydrogel in vivo is mainly due to its hemostasis of chitosan and its good tissue adhesion ability which can adhere tightly to the wound site, providing a stable gel network as a physical barrier to accelerate blood-clotting.

3.5. Antibacterial property and cell compatibility of hydrogels

The antibacterial effect of the hydrogels is important for them as wound dressing [78]. Firstly, these CSG-PEG/DMA/Zn hydrogels were contacted with bacteria to test their inherent antibacterial properties. After co-cultivation at 37 °C for 2 h, CSG-PEG hydrogel performed a low sterilization ratio, which may be due to the inherent antibacterial of CS. In contrast, there was almost no obvious bacterial colony in the hydrogel group containing zinc ions (Fig. 5a, b, and c). Quantitative results showed that the CSG-PEG/DMA3/Zn, CSG-PEG/DMA6/Zn, and CSG-PEG/DMA9/Zn hydrogels could be effective against *Staphylococcus aureus* (*S. aureus*, Gram-positive bacteria) and *Escherichia coli* (*E. coil*, Gram-negative bacteria) (Fig. 5d, f), indicating that they have excellent antibacterial properties. As the zinc ions content increases, the antibacterial property of hydrogels was enhanced. In addition, methicillin-resistant *Staphylococcus aureus* (MRSA), as a common clinically drug-resistant bacteria has also been used to evaluate the inherent antibacterial properties of CSG-PEG/DMA/Zn hydrogels [8]. As shown in Fig. 5e, CSG-PEG/DMA3/Zn, CSG-PEG/DMA6/Zn and CSG-PEG/DMA9/Zn hydrogels also had a good antibacterial effect for MRSA due to the effective antibacterial property of zinc ions [79]. A contact antibacterial test of CSG-PEG/DMA6 hydrogel (Fig. S5) was also conducted. Without the zinc ions, the inhibition ratio of the CSG-PEG/DMA6 hydrogel for *E. coil*, *S. aureus*, MRSA is only 22.7%, 28.0%, and 30.5%, indicating that zinc ions are the main antibacterial component in the hydrogel. Furthermore, the minimum inhibitory concentration (MIC) of the CSG-PEG/DMA6/Zn hydrogel was shown in Fig. S6. The OD value of the bacterial stock solution was recorded as a positive control, and the OD value of MHB was recorded as a negative control. The absorbance value of the bacterial suspension after treatment with different concentrations of materials was compared. The MIC of CSG-PEG/DMA6/Zn hydrogel for *S. aureus*, *E. coil* and MRSA were 4.0 mg/mL, 12.5 mg/mL, and 4.5 mg/mL, respectively. The release behavior of zinc ions from the hydrogel was also tested. As shown in Fig. S7, zinc ions release showed burst release performance within 1 h and the release amounts were 16.53 μg/mL, 41.6 μg/mL, and 62.5 μg/mL, respectively. Then zinc ions release rate was slowed down, and showed a sustained release within 288 h. After 288 h, the release of zinc ions from the hydrogels reached 39.3 μg/mL, 86.9 μg/mL and 118.8 μg/mL, which can provide sustained antibacterial property of the hydrogels.

The viability of L929 fibroblasts was used to evaluate the cell compatibility of these hydrogels. Firstly, the cytotoxicity of CSG-PEG/DMA/Zn hydrogels were tested by the leaching solution method. As shown in Fig. 5g, h, and i, the number of cells increased significantly within five days, which indicated that the cells grew well throughout the experiment. At the same time, there was no difference in the cell viability of different concentrations of hydrogels, and the cell viability in the cell culture medium with hydrogel extract was similar to the TCP group, indicating that these hydrogels have good cell compatibility.

Subsequently, the cytotoxicity of the materials was further evaluated by the direct contact method, and tested by co-cultivating the lyophilized hydrogel with the cells seeded on the well plate. As shown in Fig. 5j, the cytotoxicity results on 1st day indicated that with the increase of DMA and zinc ions concentration, cytotoxicity of the hydrogel showed a slight concentration-dependent changes. However, in general, different hydrogel groups all showed obvious good cell viability. After continuing to co-culture L929 cells with hydrogels from the day 1 to the day 3, it showed obvious increase of cell viability. On 3rd day, the cell viability of CSG-PEG/DMA9/Zn hydrogel had a difference compared with CSG-PEG/DMA3/Zn and CSG-PEG/DMA6/Zn (P < 0.05). Through LIVE/DEAD cell staining on 3rd day (Fig. 5k), it was found that most of the L929 cells were green and in spindle-shape and only a few of dead cells, which was consistent with the quantitative results of alamarBlue. On 5th day, CSG-PEG, CSG-PEG/DMA3/Zn, CSG-PEG/DMA6/Zn, and CSG-PEG/DMA9/Zn hydrogels were no significant difference in cell viability compared with TCP. These results showed that, consistent with the results of the leaching solution method, the hydrogels have good cell

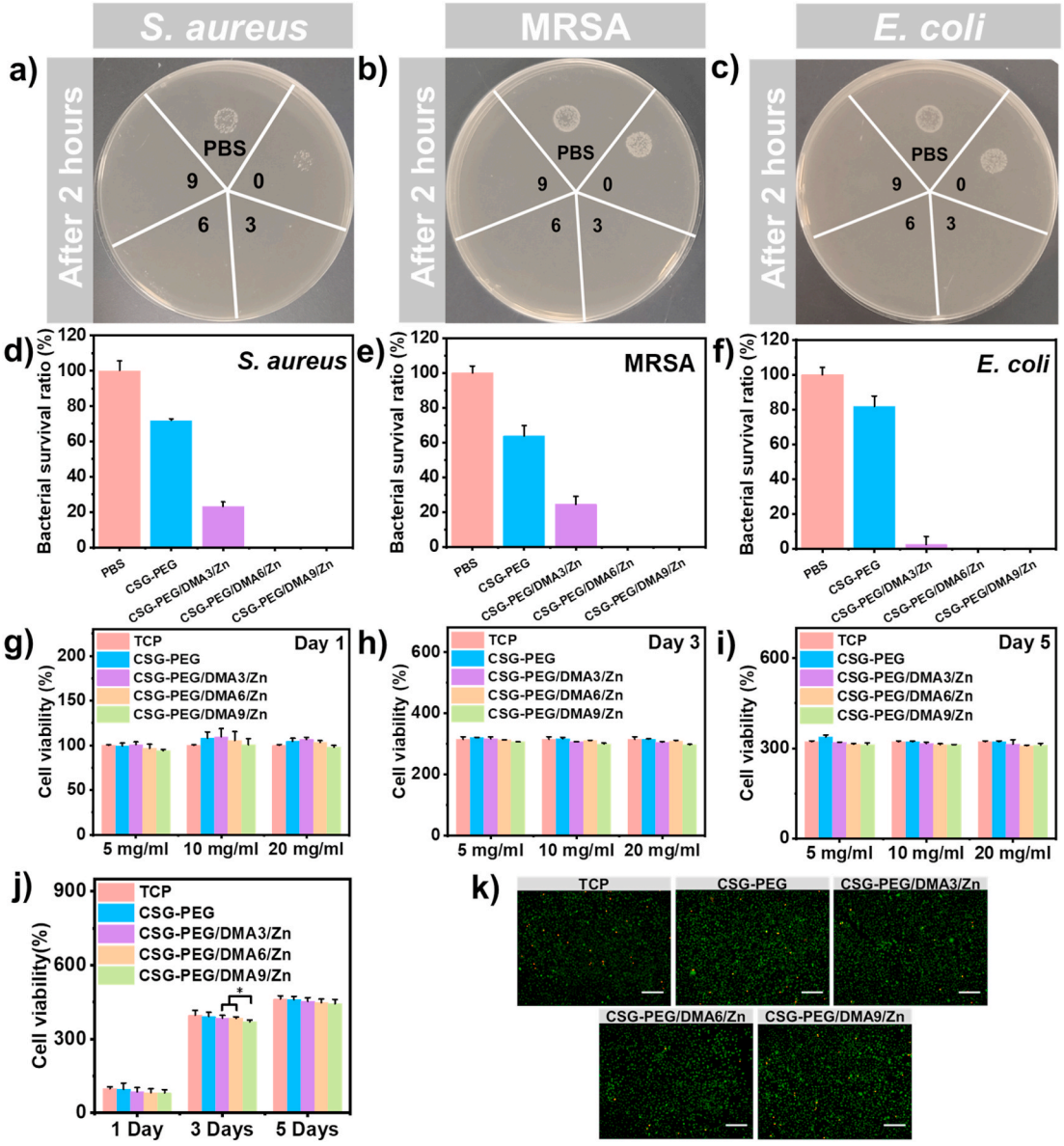

Fig. 5. Antibacterial and cell compatibility test of CSG-PEG/DMA6/Zn hydrogel. Images of contact antibacterial activity of hydrogel against (a) *S. aureus* and (b) MRSA and (c) *E. coli*; Bacterial survival ratio of *S. aureus* (d), MRSA (e), and *E. coli* (f); The cell viability on day 1 (g), day 3 (h), and day 5 (i) by using the leaching solution method; (j) The results of L929 cells survival ratio obtained by direct contact method for 1 day, 3 days, and 5 days; (k) LIVE/DEAD staining pictures of hydrogel and cells co-cultured for 72 h (n = 4).

compatibility. The cell proliferation ability of this new type hydrogels is better than our previous reported host-guest interaction hydrogels based on quaternized chitosan [46], and these hydrogels can be used as a potential candidate for clinical dressings.

3.6. *In vivo* wound healing in infected full-thickness skin defect model

All the above test results showed that CSG-PEG/DMA/Zn hydrogel can be used as a potential wound dressing for skin repair. Among them, CSG-PEG/DMA6/Zn with suitable mechanical strength, good adhesion and hemostatic ability and cell compatibility were chosen as the representative. Drug-resistant MRSA infected mouse full-thickness defect model was established to evaluate the efficacy of these hydrogels as wound dressings. Tegaderm™ Film was used as a control group. Since antibiotics was widely used to treat skin wound, CSG-PEG/DMA6 hydrogel loaded with amoxicillin (CSG-PEG/DMA6-Am) in situ was regarded as another control group. As shown in Fig. 6a, b, and c, the results showed that the wound area of all groups had a certain degree of shrinkage from 3 days to 7 days, and to 14 days. After 3 days of treatment, there was still some yellow pus at the wound site (Fig. 6a), indicating that the full-thickness skin defect model of MRSA infection was successfully established. The wound area of CSG-PEG, CSG-PEG/DMA6-Am, and CSG-PEG/DMA6/Zn hydrogel groups were significantly smaller than that of commercial Tegaderm™ Film group (Fig. 6c). The wound closure ratio of CSG-PEG/DMA6/Zn hydrogel group was approximately 25% higher than that of Tegaderm™ Film group ($P < 0.01$), which showed the best wound repair effect. The wound closure ratio of CSG-PEG and CSG-PEG/DMA6-Am hydrogel groups was similar, and also obviously higher than Tegaderm™ Film group. After 7 days of treatment, the wound closure ratio of CSG-PEG, CSG-PEG/DMA6-Am and CSG-PEG/DMA6/Zn hydrogel groups was 63%, 74%, and 86%, respectively, which showed that the wound healing effect of these hydrogels was better than Tegaderm™ Film group. Besides, the wound closure ratio of CSG-PEG/DMA6/Zn hydrogel group was significantly

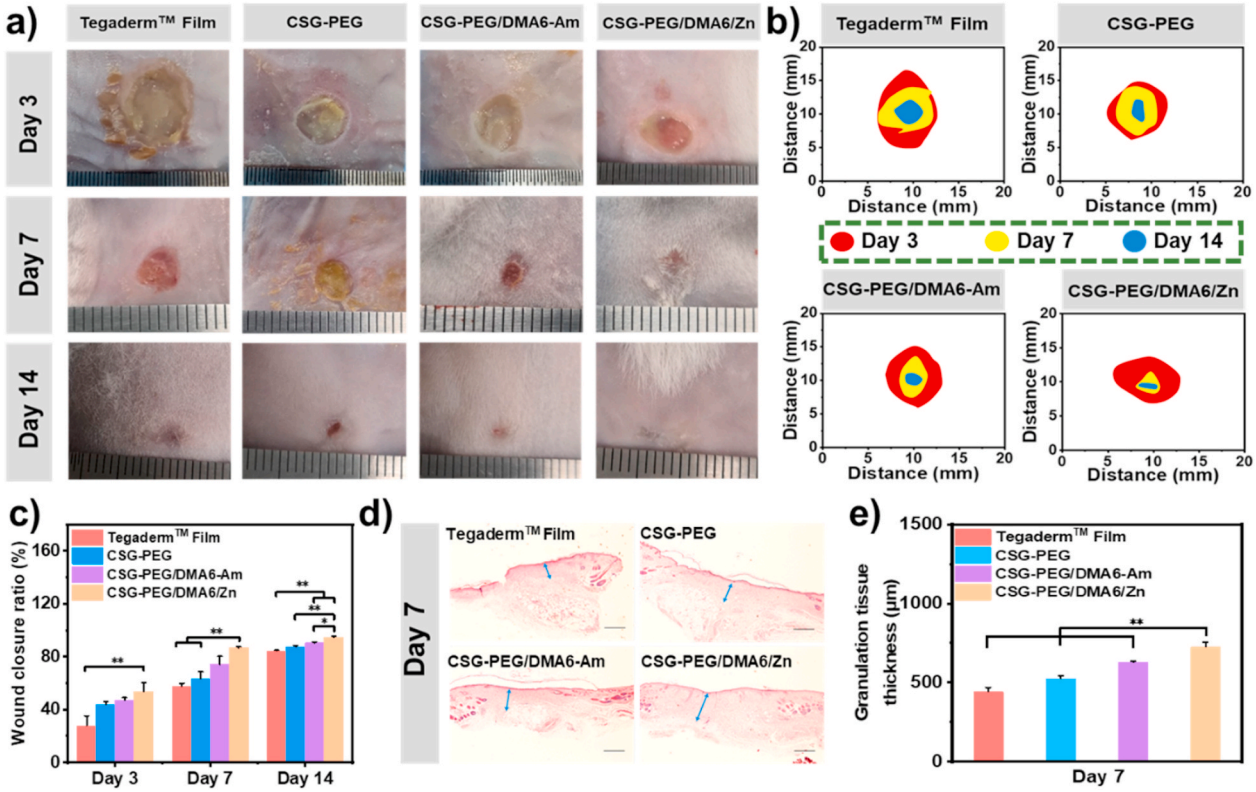

Fig. 6. (a) Images of the wound healing site on the 3rd, 7th and 14th day; (b) Schematic presentation of the wound healing site on the 3rd, 7th and 14th day; c) Statistical data of wound closure ratio (n = 5); d) Pictures of regenerating granulation tissue on the 7th day (granulation tissue: blue arrows), scale bar: 400 μm; e) The results of the thickness of the regenerated granulation tissue on the 7th day (n = 5). *P < 0.05, **P < 0.01.

higher than that of Tegaderm ™ Film group and CSG-PEG hydrogel group (P < 0.01). More importantly, the wound closure rate of the CSG-PEG/DMA6/Zn hydrogel group on day 7 was better than that of the other repeorted mPEG-modified chitosan-based hydrogel [26], which is because zinc ions provided the antibacterial effect in the initial stage of infection, and promoted the migration of fibroblasts and vascular remodeling during the wound healing stage. On the 14th day, the wound in the CSG-PEG/DMA6/Zn group was almost completely healed (wound closure ratio was more than 95%). The residual area of the wound in the CSG-PEG/DMA6-Am hydrogel was only 10%, and amount of wound area remained more than 10% in the other groups.

Granulation tissue is composed of newly formed capillaries and proliferated fibroblasts, which play a critical role in wound repair [4]. Therefore, the thickness of granulation tissue was measured to distinguish the quality of wound repair. As shown in Fig. 6d and e, after 7 days of healing, Tegaderm™ Film showed the thinnest granulation tissue thickness (441 μm). The granulation tissue thickness of CSG-PEG and CSG-PEG/DMA6-Am, and CSG-PEG/DMA6/Zn hydrogel were 527 μm, and 628 μm, and 724 μm, respectively, and 724 μm was significantly thicker than other groups (P < 0.01). All these results indicated the best effects of CSG-PEG/DMA6/Zn hydrogel in the wound healing process. In conclusion, the hydrogel containing dopamine and zinc ions showed the best treatment effect in entire wound healing stage. This is because dopamine can effectively remove ROS and prevent peroxidation damage at the wound site, and zinc ions can not only effectively kill bacterium, but also promote the proliferation and migration of fibroblasts, which contributes to the formation of epithelial tissue [17,20,80]. In general, CSG-PEG/DMA6/Zn hydrogel is superior to the commercial Tegaderm™ Film due to its inherent antibacterial and wound healing ability.

3.7. Histomorphological evaluation

Wound healing is a complex and orderly physiological process, which includes hemostasis, inflammation, migration, proliferation and remodeling [81]. Hematoxylin and eosin stained sections (H&E staining) were used to evaluate the wound healing effect at different stages [82]. As shown in Fig. 7a, all the hydrogel groups showed mild inflammatory response after 3 days of treatment, but Tegaderm™ Film group showed strong acute inflammation. Besides, compared with the CSG-PEG and CSG-PEG/DMA6-Am hydrogel groups, the CSG-PEG/DMA6/Zn hydrogel group showed relatively fewer inflammatory cells and more fibroblasts. This may be due to the antioxidant ability of dopamine, and zinc ions' promotion of migration of fibroblasts [20]. On the 7th day, all the groups almost formed varied degrees of epidermal structure, and had a large number of migrated fibroblasts. Compared with Tegaderm™ Film and CSG-PEG, CSG-PEG/DMA6-Am and CSG-PEG/DMA6/Zn hydrogel groups had relatively thicker epidermis.

New blood vessels provide nutrients and oxygen for wound site, which is essential for wound repairing [83]. The number of blood vessels at the wound site was counted on the 7th day to evaluate wound healing effect (Fig. 7c), and the results showed that the CSG-PEG/DMA6/Zn hydrogel group revealed the best angiogenesis promotion effect (Fig. 7a, pointed by the red arrow), which was significantly higher than Tegaderm™ Film group (P < 0.01) and CSG-PEG hydrogel group (P < 0.05). This is due to the function of zinc ions to promote angiogenesis [80]. On the 14th day, although the Tegaderm™ Film group showed complete epithelial regeneration, but still no obvious hair follicle formation. In contrast, the hydrogel treatment groups, especially epidermal structure of the CSG-PEG/DMA6/Zn hydrogel group appeared similar to the normal tissues, and there was more skin component such as hair follicles (Fig. 7a, pointed by the green arrow). The statistical results

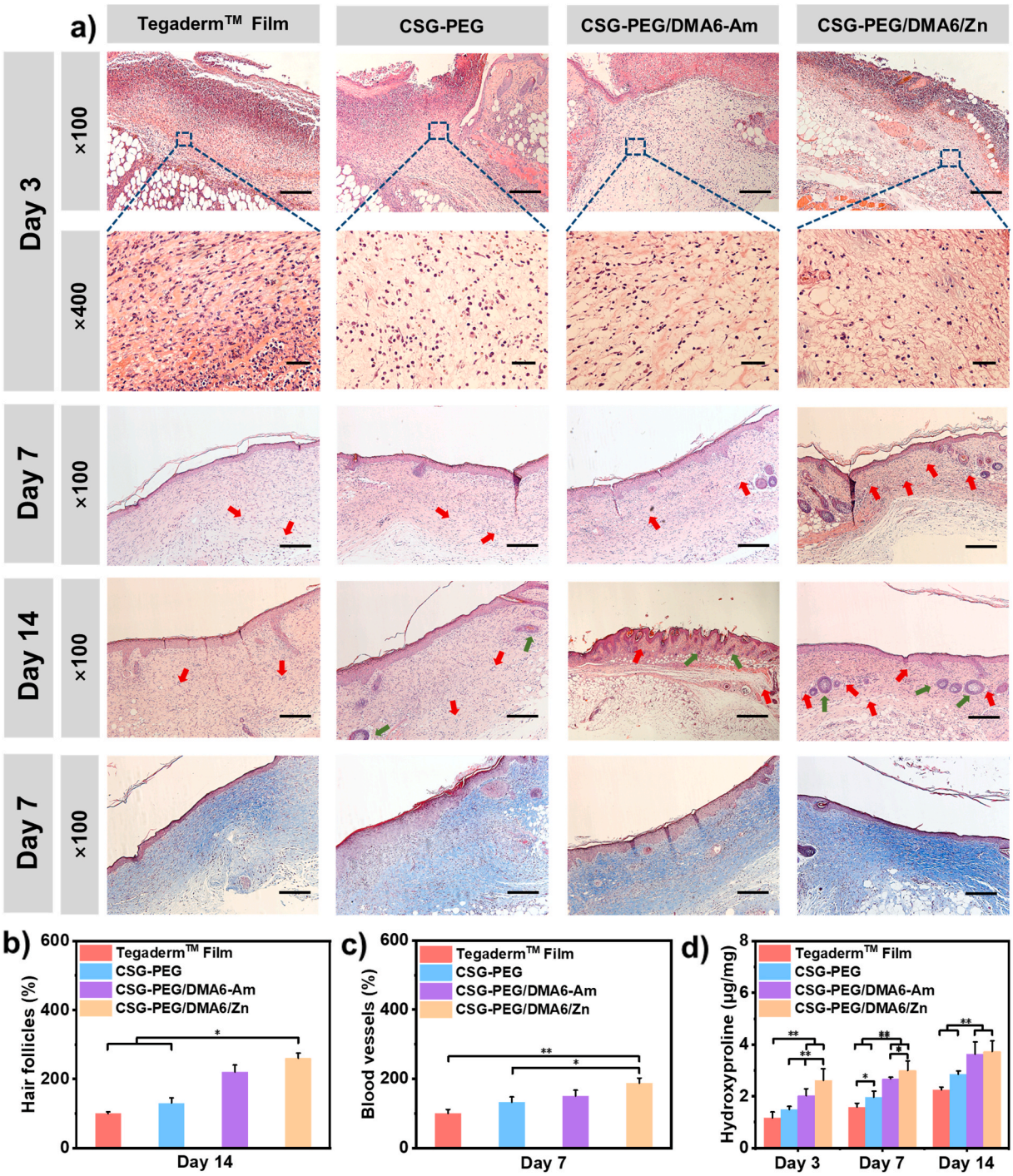

Fig. 7. (a) Morphological results of wound healing site after treatment for 3 days, 7 days and 14 days, and Masson's trichrome staining at the wound site on the 7th day, scale bar: 200 μm; (b) Newborn hair follicles on 14th day; (c) Regeneration of blood vessels on 7th day; (d) Collagen amount by measuring the content of hydroxyproline. *P < 0.05, **P < 0.01.

showed that the number of hair follicle regeneration in CSG-PEG/DMA6/Zn hydrogel group was significantly higher than that in Tegaderm™ Film ($P < 0.05$) and CSG-PEG hydrogel group ($P < 0.05$) (Fig. 7b). However, CSG-PEG/DMA6-Am hydrogel group occurred a certain degree of irregular epidermis on the 14th day, which indicated that wound healing effect of CSG -PEG/DMA6-Am hydrogel was not very satisfactory. These results indicated that the CSG-PEG/DMA6/Zn hydrogel exhibits the best effect on extracellular matrix remodeling and tissue regeneration.

3.8. Analysis of collagen deposition in wound healing

The process of wound healing always accompanied by changes in collagen metabolism. Hydroxyproline is the most widely distributed key component of collagen (content is 13.4%) [46], and the amount of hydroxyproline can reflect the collagen metabolism of wound site [84]. The total collagen level in granulation tissue was tested by analyzing the content of hydroxyproline to evaluate the effects of the four treatments groups. As shown in Fig. 7d, on the 3rd day, CSG-PEG/DMA6/Zn hydrogel group showed the most collagen deposition compared with

other groups (P < 0.01). The amount of collagen deposition of CSG-PEG/DMA6/Zn hydrogel group was significantly higher than that in the CSG-PEG/DMA-Am hydrogel group on the 7th day (P < 0.05). On the 14th day, the collagen deposition of CSG-PEG/DMA6/Zn hydrogel group and CSG-PEG/DMA6-Am hydrogel group was similar, which was still significantly higher than that of Tegaderm™ Film group and CSG-PEG hydrogel group (P < 0.01). Within 14 days of treatment, the collagen content in the wound site continued to increase. Compared with the Tegaderm™ Film group, the hydrogel groups showed a better collagen deposition throughout the repairing process. At the same time, Masson's trichrome staining was performed on the tissue section on the 7th day to observe collagen deposition (Fig. 7a). The collagen in the wound treated was dyed blue. Compared with Tegaderm™ Film group, the hydrogel treatment groups exhibited more blue color, and the CSG-PEG/DMA6/Zn group showed the best collagen regeneration ability compared with other hydrogel groups. Therefore, these results proved that the CSG-PEG/DMA6/Zn hydrogel can effectively promote collagen deposition.

3.9. The expression of CD31 and CD68 during wound healing

Many studies have shown that cytokine changes during wound healing are closely related to cell metabolism and proliferation [85,86]. CD68 is ubiquitous in monocytes and macrophages, especially near the wounds [87]. CD68 is highly expressed in inflammation, as the level of inflammation decreases, the expression of CD68 decreases [88]. CD31 plays an important role in vascular regeneration for the proliferation and remolding stage of wound healing, and is used to evaluate the neovascularization during wound healing [89]. Therefore, CD68 and CD31 were selected as indicators to evaluate the inflammation and angiogenesis of wound healing process for wound dressing. The immunofluorescence staining of CD68 (Fig. 8a) and the quantitative results (Fig. 8b) showed that the expression of CD68 is higher in the inflammation stage, and the expression level gradually decreases over time during the whole process of wound healing. On the 3rd day and 7th day, compared with other groups, the CSG-PEG/DMA6/Zn hydrogel group showed the lowest CD68 expression (P < 0.05), which was mainly

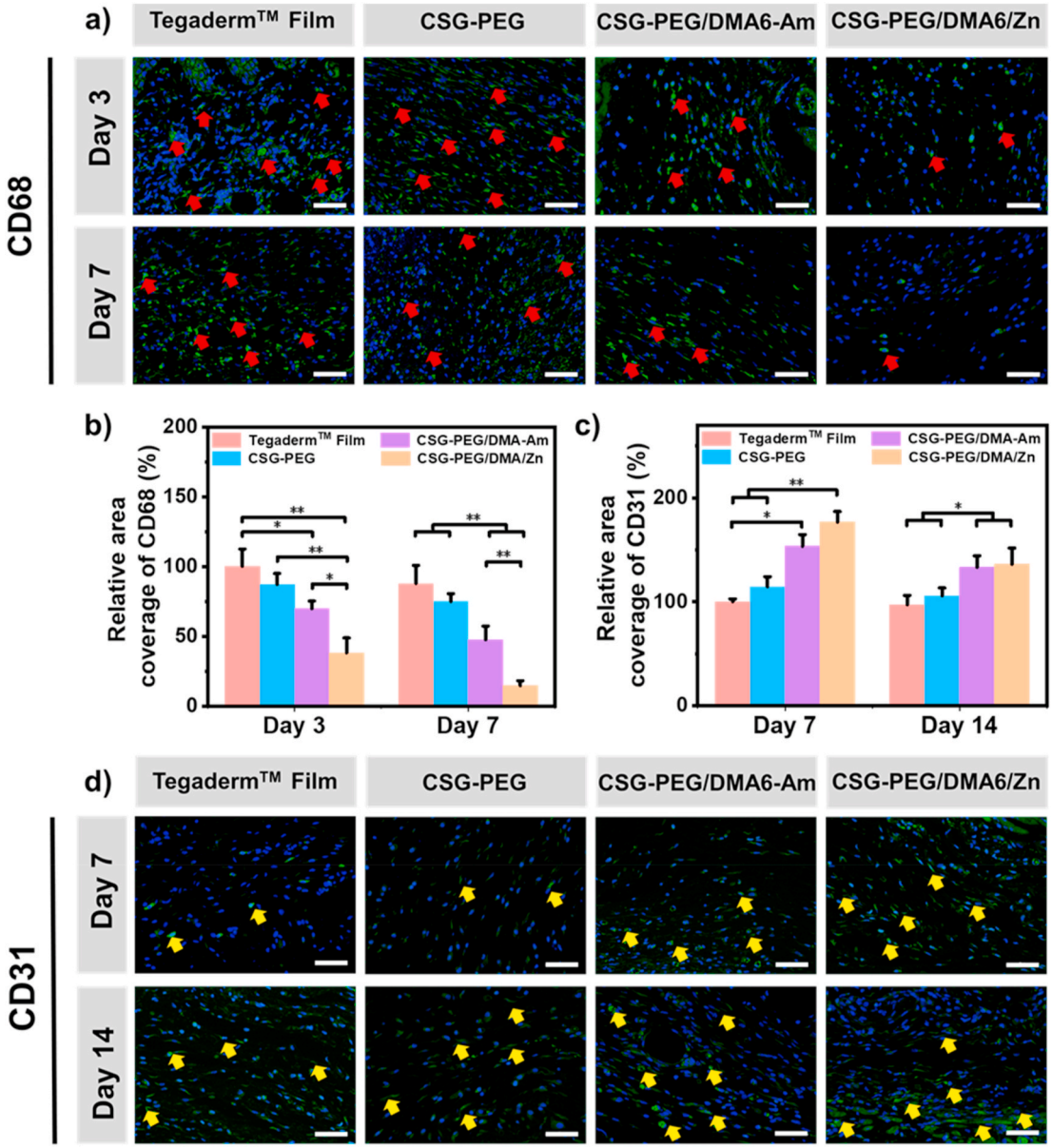

Fig. 8. Immunofluorescence staining results of wound regeneration site on 3rd day and 7th day with (a) CD68 and on 7th day and 14th day with (d) CD31. Red arrows indicate the expression of CD68, and yellow arrows indicate CD31, scale bar: 50 μm; Quantitative results of (b) CD68 and (c) CD31 relative area ratio (n = 3). For all quantitative data, the data of the commercial film groups on the 3rd day of CD68 and the 7th day of CD31 were taken as 100%. *P < 0.05, **P < 0.01.

because the zinc ion is antibacterial and can promote fibroblast proliferation. The immunofluorescence staining of CD31 and quantitative results are shown in Fig. 8c and d. Compared with Tegaderm™ Film, CSG-PEG and CSG-PEG/DMA-Am, the wound site treated with CSG-PEG/DMA6/Zn hydrogel showed more CD31 expression on the 7th day. In addition, on the 14th day, the expression levels of CD31 in the CSG-PEG/DMA-Am hydrogel group and the CSG-PEG/DMA6/Zn hydrogel group were similar and significantly higher than Tegaderm™ Film group ($P < 0.05$). In short, by reducing the expression of CD68 and simultaneously promoting the expression of CD31, CSG-PEG/DMA6/Zn hydrogel can significantly promote wound healing and has a better repair effect than Tegaderm™ Film.

4. Conclusions

In this work, we developed a series of multifunctional hydrogels with antibacterial properties, compressibility, adhesion, antioxidation and hemostasis, and further demonstrated that they can be used as a new type of drug-resistant bacteria infected skin wound dressing. These hydrogels showed stable rheological property, short gelation time, excellent tissue adhesion, biocompatibility, antibacterial property and free radical scavenging capability, which can effectively promote wound healing. In addition, the CSG-PEG/DMA6/Zn hydrogel showed good blood-clotting ability in vitro and hemostatic ability in vivo. Compared with Tegaderm™ Film and PEG-CSG and PEG-CSG/DMA-Am, CSG-PEG/DMA6/Zn hydrogels showed the excellent therapeutic effect in term of the wound closure ratio, granulation tissue regeneration and collagen deposition in the full-thickness skin defect model of MRSA infection. In addition, the results of CD31 and CD68 staining during the wound healing process further showed that these multifunctional hydrogels have effective promotion in the wound healing process by reducing inflammation and promoting vascular regeneration. All results indicate that these multifunctional antibiotic-independent antibacterial adhesion antioxidant hemostasis hydrogels represent competitive candidates and can be used to treat wounds infected by resistant bacteria.

CRediT authorship contribution statement

Yutong Yang: Formal analysis, Writing – original draft, Methodology. **Yongping Liang:** Conducted most of the animal experiments, Formal analysis. **Jueying Chen:** Conducted the antibacterial test, Formal analysis. **Xianglong Duan:** Writing – review & editing, Project administration, Funding acquisition. **Baolin Guo:** Conceptualization, Methodology, Writing – review & editing, Supervision, Funding acquisition.

Declaration of competing interest

The authors declare that they have no competing interests.

Acknowledgments

This work was jointly supported by the National Natural Science Foundation of China (grant numbers: 51973172, and 51673155), the Natural Science Foundation of Shaanxi Province (No. 2020JC-03 and 2019TD-020), State Key Laboratory for Mechanical Behavior of Materials, and the Fundamental Research Funds for the Central Universities, and the World-Class Universities (Disciplines) and the Characteristic Development Guidance Funds for the Central Universities, and Opening Project of Key Laboratory of Shaanxi Province for Craniofacial Precision Medicine Research, College of Stomatology, Xi'an Jiaotong University (No. 2019LHM-KFKT008), and the Key R&D Program of Shaanxi Province (No. 2019ZDLSF02-09-01, 2020GXLH-Y-019), Innovation Capability Support Program of Shaanxi Province (Program No. 2019GHJD-14, 2021TD-40), and Scientific Research Program Funded by Shaanxi Provincial Education Department (ProgramNo.18JC027).

Appendix A. Supplementary data

Supplementary data to this article can be found online at https://doi.org/10.1016/j.bioactmat.2021.06.014.

References

[1] N. Annabi, D. Rana, E. Shirzaei Sani, R. Portillo-Lara, J.L. Gifford, M.M. Fares, S. M. Mithieux, A.S. Weiss, Engineering a sprayable and elastic hydrogel adhesive with antimicrobial properties for wound healing, Biomaterials 139 (2017) 229–243.
[2] M. Li, Y. Liang, J. He, H. Zhang, B. Guo, Two-pronged strategy of biomechanically active and biochemically multifunctional hydrogel wound dressing to accelerate wound closure and wound healing, Chem. Mater. 32 (2020) 9937–9953.
[3] J. He, Y. Liang, M. Shi, B. Guo, Anti-oxidant electroactive and antibacterial nanofibrous wound dressings based on poly(ε-caprolactone)/quaternized chitosan-graft-polyaniline for full-thickness skin wound healing, Chem. Eng. J. 385 (2020) 123464.
[4] J. He, M. Shi, Y. Liang, B. Guo, Conductive adhesive self-healing nanocomposite hydrogel wound dressing for photothermal therapy of infected full-thickness skin wounds, Chem. Eng. J. 394 (2020) 124888.
[5] C. Hu, F. Zhang, Q. Kong, Y. Lu, B. Zhang, C. Wu, R. Luo, Y. Wang, Synergistic chemical and photodynamic antimicrobial therapy for enhanced wound healing mediated by multifunctional light-responsive nanoparticles, Biomacromolecules 20 (2019) 4581–4592.
[6] S. Li, M. Pei, T. Wan, H. Yang, S. Gu, Y. Tao, X. Liu, Y. Zhou, W. Xu, P. Xiao, Self-healing hyaluronic acid hydrogels based on dynamic Schiff base linkages as biomaterials, Carbohydr. Polym. 250 (2020) 116922.
[7] Z. Li, F. Zhou, Z. Li, S. Lin, L. Chen, L. Liu, Y. Chen, Hydrogel cross-linked with dynamic covalent bonding and micellization for promoting burn wound healing, ACS Appl. Mater. Interfaces 10 (2018) 25194–25202.
[8] Y. Liang, B. Chen, M. Li, J. He, Z. Yin, B. Guo, Injectable Antimicrobial conductive hydrogels for wound disinfection and infectious wound healing, Biomacromolecules 21 (2020) 1841–1852.
[9] C. Qi, L. Xu, Y. Deng, G. Wang, Z. Wang, L. Wang, Sericin hydrogels promote skin wound healing with effective regeneration of hair follicles and sebaceous glands after complete loss of epidermis and dermis, Biomater. Sci. 6 (2018) 2859–2870.
[10] X. Zhao, M. Zhang, B. Guo, P.X. Ma, Mussel-inspired injectable supramolecular and covalent bond crosslinked hydrogels with rapid self-healing and recovery properties via a facile approach under metal-free conditions, J. Mater. Chem. B 4 (2016) 6644–6651.
[11] J. Currie, W. Lin, W. Zhang, Patient knowledge and antibiotic abuse: evidence from an audit study in China, J. Health Econ. 30 (2011) 933–949.
[12] J. Zhang, J. Ge, Y. Xu, J. Chen, A. Zhou, L. Sun, Y. Gao, Y. Zhang, T. Gu, X. Ning, Bioactive multi-engineered hydrogel offers simultaneous promise against antibiotic resistance and wound damage, Int. J. Biol. Macromol. 164 (2020) 4466–4474.
[13] X. Zhao, Y. Liang, Y. Huang, J. He, Y. Han, B. Guo, Physical double-network hydrogel adhesives with rapid shape adaptability, fast self-healing, antioxidant and NIR/pH stimulus-responsiveness for multidrug-resistant bacterial infection and removable wound dressing, Adv. Funct. Mater. 30 (2020) 1910748.
[14] S. Ahtzaz, M. Nasir, L. Shahzadi, W. Amir, A. Anjum, R. Arshad, F. Iqbal, A. A. Chaudhry, M. Yar, I.u. Rehman, A study on the effect of zinc oxide and zinc peroxide nanoparticles to enhance angiogenesis-pro-angiogenic grafts for tissue regeneration applications, Mater, DES 132 (2017) 409–418.
[15] H. Chen, J. Cheng, L. Ran, K. Yu, B. Lu, G. Lan, F. Dai, F. Lu, An injectable self-healing hydrogel with adhesive and antibacterial properties effectively promotes wound healing, Carbohydr. Polym. 201 (2018) 522–531.
[16] X. Du, Y. Hou, L. Wu, S. Li, A. Yu, D. Kong, L. Wang, G. Niu, An anti-infective hydrogel adhesive with non-swelling and robust mechanical properties for sutureless wound closure, J. Mater. Chem. B 8 (2020) 5682–5693.
[17] Y. Gao, Y. Han, M. Cui, H.L. Tey, L. Wang, C. Xu, ZnO nanoparticles as an antimicrobial tissue adhesive for skin wound closure, J. Mater. Chem. B 5 (2017) 4535–4541.
[18] W. Han, B. Zhou, K. Yang, X. Xiong, S. Luan, Y. Wang, Z. Xu, P. Lei, Z. Luo, J. Gao, Y. Zhan, G. Chen, L. Liang, R. Wang, S. Li, H. Xu, Biofilm-inspired adhesive and antibacterial hydrogel with tough tissue integration performance for sealing hemostasis and wound healing, Bioactive Mater. 5 (2020) 768–778.
[19] H. Cheng, K. Yue, M. Kazemzadeh-Narbat, Y. Liu, A. Khalilpour, B. Li, Y.S. Zhang, N. Annabi, A. Khademhosseini, Mussel-Inspired multifunctional hydrogel coating for prevention of infections and enhanced osteogenesis, ACS Appl. Mater. Interfaces 9 (2017) 11428–11439.
[20] Y. Li, X. Liu, L. Tan, Z. Cui, X. Yang, Y. Zheng, K.W.K. Yeung, P.K. Chu, S. Wu, Rapid sterilization and accelerated wound healing using Zn2+ and graphene oxide modified g-C3N4 under dual light irradiation, Adv. Funct. Mater. 28 (2018) 1800299.
[21] T. Majima, W. Schnabel, W. Weber, Phenyl-2,4,6-Trimethylbenzoylphosphinates as water-soluble photoinitiators - generation and reactivity of O=P(C6h5)(O-) radical-anions, Makromolekulare Chemie-Macromolecular Chemistry and Physics 192 (1991) 2307–2315.
[22] X. Du, Y. Liu, H. Yan, M. Rafique, S. Li, X. Shan, L. Wu, M. Qiao, D. Kong, L. Wang, Anti-Infective and pro-coagulant chitosan-based hydrogel tissue adhesive for sutureless wound closure, Biomacromolecules 21 (2020) 1243–1253.
[23] N. Bhattarai, J. Gunn, M. Zhang, Chitosan-based hydrogels for controlled, localized drug delivery, Adv. Drug Deliv. Rev. 62 (2010) 83–99.

[24] M.S. Sarwar, A. Ghaffar, Q. Huang, M.S. Zafar, M. Usman, M. Latif, Controlled-release behavior of ciprofloxacin from a biocompatible polymeric system based on sodium alginate/poly(ethylene glycol) mono methyl ether, Int. J. Biol. Macromol. 165 (2020) 1047–1054.
[25] T. Ito, C. Yoshida, Y. Murakami, Design of novel sheet-shaped chitosan hydrogel for wound healing: a hybrid biomaterial consisting of both PEG-grafted chitosan and crosslinkable polymeric micelles acting as drug containers, Mater. Sci. Eng. C 33 (2013) 3697–3703.
[26] D.H. Yang, D.I. Seo, D.-W. Lee, S.H. Bhang, K. Park, G. Jang, C.H. Kim, H.J. Chun, Preparation and evaluation of visible-light cured glycol chitosan hydrogel dressing containing dual growth factors for accelerated wound healing, J. Ind. Eng. Chem. 53 (2017) 360–370.
[27] J. Zhu, F. Li, X. Wang, J. Yu, D. Wu, Hyaluronic acid and polyethylene glycol hybrid hydrogel encapsulating nanogel with hemostasis and sustainable antibacterial property for wound healing, ACS Appl. Mater. Interfaces 10 (2018) 13304–13316.
[28] V. Mouriño, J.P. Cattalini, A.R. Boccaccini, Metallic ions as therapeutic agents in tissue engineering scaffolds: an overview of their biological applications and strategies for new developments, J. R. Soc. Interface 9 (2012) 401–419.
[29] Y. Shi, M. Liu, F. Deng, G. Zeng, Q. Wan, X. Zhang, Y. Wei, Recent progress and development on polymeric nanomaterials for photothermal therapy: a brief overview, J. Mater. Chem. B 5 (2017) 194–206.
[30] A. Sirelkhatim, S. Mahmud, A. Seeni, N.H.M. Kaus, L.C. Ann, S.K.M. Bakhori, H. Hasan, D. Mohamad, Review on zinc oxide nanoparticles: antibacterial activity and toxicity mechanism, Nano-Micro Lett. 7 (2015) 219–242.
[31] C. Mao, Y. Xiang, X. Liu, Z. Cui, X. Yang, K.W.K. Yeung, H. Pan, X. Wang, P.K. Chu, S. Wu, Photo-Inspired antibacterial activity and wound healing acceleration by hydrogel embedded with Ag/Ag@AgCl/ZnO nanostructures, ACS Nano 11 (2017) 9010–9021.
[32] Z. Bao, X. Liu, Y. Liu, H. Liu, K. Zhao, Near-infrared light-responsive inorganic nanomaterials for photothermal therapy, Asian J. Pharm. Sci. 11 (2016) 349–364.
[33] P.G. Jamkhande, N.W. Ghule, A.H. Bamer, M.G. Kalaskar, Metal nanoparticles synthesis: an overview on methods of preparation, advantages and disadvantages, and applications, J. Drug Deliv. Sci. Technol. 53 (2019) 101174.
[34] N.R. Brun, M. Lenz, B. Wehrli, K. Fent, Comparative effects of zinc oxide nanoparticles and dissolved zinc on zebrafish embryos and eleuthero-embryos: importance of zinc ions, Sci. Total Environ. 476–477 (2014) 657–666.
[35] G. Applerot, A. Lipovsky, R. Dror, N. Perkas, Y. Nitzan, R. Lubart, A. Gedanken, Enhanced antibacterial activity of nanocrystalline ZnO due to increased ROS-mediated cell injury, Adv. Funct. Mater. 19 (2009) 842–852.
[36] D.E. Fullenkamp, J.G. Rivera, Y.-k. Gong, K.H.A. Lau, L. He, R. Varshney, P. B. Messersmith, Mussel-inspired silver-releasing antibacterial hydrogels, Biomaterials 33 (2012) 3783–3791.
[37] D. Gan, T. Xu, W. Xing, X. Ge, L. Fang, K. Wang, F. Ren, X. Lu, Mussel-Inspired contact-active antibacterial hydrogel with high cell affinity, toughness, and recoverability, Adv. Funct. Mater. 29 (2019) 1805964.
[38] X. He, X. Liu, J. Yang, H. Du, N. Chai, Z. Sha, M. Geng, X. Zhou, C. He, Tannic acid-reinforced methacrylated chitosan/methacrylated silk fibroin hydrogels with multifunctionality for accelerating wound healing, Carbohydr. Polym. 247 (2020) 116689.
[39] Y. Liang, Z. Li, Y. Huang, R. Yu, B. Guo, Dual-Dynamic-bond cross-linked antibacterial adhesive hydrogel sealants with on-demand removability for post-wound-closure and infected wound healing, ACS Nano 15 (2021) 7078–7093.
[40] M. Puertas-Bartolomé, L. Benito-Garzón, S. Fung, J. Kohn, B. Vázquez-Lasa, J. San Román, Bioadhesive functional hydrogels: controlled release of catechol species with antioxidant and antiinflammatory behavior, Mater. Sci. Eng. C 105 (2019) 110040.
[41] T. Wang, X.Y. Mu, H.B. Li, W.L. Wu, J. Nie, D.Z. Yang, The photocrosslinkable tissue adhesive based on copolymeric dextran/HEMA, Carbohydr. Polym. 92 (2013) 1423–1431.
[42] J. Hu, Y. Hou, H. Park, B. Choi, S. Hou, A. Chung, M. Lee, Visible light crosslinkable chitosan hydrogels for tissue engineering, Acta Biomater. 8 (2012) 1730–1738.
[43] R. Mathiyalagan, Y.J. Kim, C. Wang, Y. Jin, S. Subramaniyam, P. Singh, D. Wang, D.C. Yang, Protopanaxadiol aglycone ginsenoside-polyethylene glycol conjugates: synthesis, physicochemical characterizations, and in vitro studies, Artif. Cell Nanomed. B 44 (2016) 1803–1809.
[44] S. Hou, P.X. Ma, Stimuli-Responsive supramolecular hydrogels with high extensibility and fast self-healing via precoordinated mussel-inspired chemistry, Chem. Mater. 27 (2015) 7627–7635.
[45] J. Qu, X. Zhao, P.X. Ma, B. Guo, Injectable antibacterial conductive hydrogels with dual response to an electric field and pH for localized “smart” drug release, Acta Biomater. 72 (2018) 55–69.
[46] B. Zhang, J. He, M. Shi, Y. Liang, B. Guo, Injectable self-healing supramolecular hydrogels with conductivity and photo-thermal antibacterial activity to enhance complete skin regeneration, Chem. Eng. J. 400 (2020) 125994.
[47] E. Shirzaei Sani, R. Portillo Lara, Z. Aldawood, S.H. Bassir, D. Nguyen, A. Kantarci, G. Intini, N. Annabi, An antimicrobial dental light curable bioadhesive hydrogel for treatment of peri-implant diseases, Matter 1 (2019) 926–944.
[48] Y. Liang, X. Zhao, T. Hu, B. Chen, Z. Yin, P.X. Ma, B. Guo, Adhesive hemostatic conducting injectable composite hydrogels with sustained drug release and photothermal antibacterial activity to promote full-thickness skin regeneration during wound healing, Small 15 (2019) 1900046.
[49] Y. Huang, X. Zhao, Z. Zhang, Y. Liang, Z. Yin, B. Chen, L. Bai, Y. Han, B. Guo, Degradable gelatin-based IPN cryogel hemostat for rapidly stopping deep noncompressible hemorrhage and simultaneously improving wound healing, Chem. Mater. 32 (2020) 6595–6610.
[50] X. Zhao, P. Li, B. Guo, P.X. Ma, Antibacterial and conductive injectable hydrogels based on quaternized chitosan-graft-polyaniline/oxidized dextran for tissue engineering, Acta Biomater. 26 (2015) 236–248.
[51] M. Zhang, S. Chen, L. Zhong, B. Wang, H. Wang, F. Hong, Zn2+-loaded TOBC nanofiber-reinforced biomimetic calcium alginate hydrogel for antibacterial wound dressing, Int. J. Biol. Macromol. 143 (2020) 235–242.
[52] M. Shu, S. Long, Y. Huang, D. Li, H. Li, X. Li, High strength and antibacterial polyelectrolyte complex CS/HS hydrogel films for wound healing, Soft Matter 15 (2019) 7686–7694.
[53] T. Dai, M. Tanaka, Y.-Y. Huang, M.R. Hamblin, Chitosan preparations for wounds and burns: antimicrobial and wound-healing effects, Expert Rev. Anti Infect. Ther. 9 (2011) 857–879.
[54] X. Huang, Y. Sun, J. Nie, W. Lu, L. Yang, Z. Zhang, H. Yin, Z. Wang, Q. Hu, Using absorbable chitosan hemostatic sponges as a promising surgical dressing, Int. J. Biol. Macromol. 75 (2015) 322–329.
[55] A. Verlee, S. Mincke, C.V. Stevens, Recent developments in antibacterial and antifungal chitosan and its derivatives, Carbohydr. Polym. 164 (2017) 268–283.
[56] T. Furuike, D. Komoto, H. Hashimoto, H. Tamura, Preparation of chitosan hydrogel and its solubility in organic acids, Int. J. Biol. Macromol. 104 (2017) 1620–1625.
[57] A. Zubareva, B. Shagdarova, V. Varlamov, E. Kashirina, E. Svirshchevskaya, Penetration and toxicity of chitosan and its derivatives, Eur. Polym. J. 93 (2017) 743–749.
[58] H. Xu, D. Zhang, J. Li, Antibacterial nanoparticles with universal adhesion function based on dopamine and eugenol, J. Bioresour. Bioprod. 4 (2019) 177–182.
[59] Y.-I. Jeong, D.-G. Kim, M.-K. Jang, J.-W. Nah, Preparation and spectroscopic characterization of methoxy poly(ethylene glycol)-grafted water-soluble chitosan, Carbohydr. Res. 343 (2008) 282–289.
[60] M. He, C.-C. Chu, Dual stimuli responsive glycidyl methacrylate chitosan-quaternary ammonium hybrid hydrogel and its bovine serum albumin release, J. Appl. Polym. Sci. 130 (2013) 3736–3745.
[61] Y. Hong, Y. Xi, J. Zhang, D. Wang, H. Zhang, N. Yan, S. He, J. Du, Polymersome–hydrogel composites with combined quick and long-term antibacterial activities, J. Mater. Chem. B 6 (2018) 6311–6321.
[62] I.W.G.o.R.o.S. Cancer, E.t.A.U.L. Meeting, Exposure to Artificial UV Radiation and Skin Cancer, Exposure to Artificial UV Radiation and Skin Cancer, 2006.
[63] R. Wang, B. Zhou, D.-l. Xu, H. Xu, L. Liang, X.-h. Feng, P.-k. Ouyang, B. Chi, Antimicrobial and biocompatible ε-polylysine–γ-poly(glutamic acid)–based hydrogel system for wound healing, J. Bioact. Compat Polym. 31 (2016) 242–259.
[64] Z. Zhang, X. Wang, Y. Wang, J. Hao, Rapid-forming and self-healing agarose-based hydrogels for tissue adhesives and potential wound dressings, Biomacromolecules 19 (2018) 980–988.
[65] Y.P. Liang, X. Zhao, T.L. Hu, Y. Han, B.L. Guo, Mussel-inspired, antibacterial, conductive, antioxidant, injectable composite hydrogel wound dressing to promote the regeneration of infected skin, J. Colloid Interface Sci. 556 (2019) 514–528.
[66] Q. Tang, C. Chen, Y. Jiang, J. Huang, Y. Liu, P.M. Nthumba, G. Gu, X. Wu, Y. Zhao, J. Ren, Engineering an adhesive based on photosensitive polymer hydrogels and silver nanoparticles for wound healing, J. Mater. Chem. B 8 (2020) 5756–5764.
[67] J. Yang, J. Keijsers, M. van Heek, A. Stuiver, M.A. Cohen Stuart, M. Kamperman, The effect of molecular composition and crosslinking on adhesion of a bio-inspired adhesive, Polym. Chem. 6 (2015) 3121–3130.
[68] W. Zhang, R. Wang, Z. Sun, X. Zhu, Q. Zhao, T. Zhang, A. Cholewinski, F. Yang, B. Zhao, R. Pinnaratip, P.K. Forooshani, B.P. Lee, Catechol-functionalized hydrogels: biomimetic design, adhesion mechanism, and biomedical applications, Chem. Soc. Rev. 49 (2020) 433–464.
[69] J. Qu, X. Zhao, Y. Liang, T. Zhang, P.X. Ma, B. Guo, Antibacterial adhesive injectable hydrogels with rapid self-healing, extensibility and compressibility as wound dressing for joints skin wound healing, Biomaterials 183 (2018) 185–199.
[70] H. Li, Q. Xu, Y. Chen, A. Wan, Effect of concentration and molecular weight of chitosan and its derivative on the free radical scavenging ability, J. Biomed. Mater. Res. 102 (2014) 911–916.
[71] C. Liu, C. Liu, S. Yu, N. Wang, W. Yao, X. Liu, G. Sun, Q. Song, W. Qiao, Efficient antibacterial dextran-montmorillonite composite sponge for rapid hemostasis with wound healing, Int. J. Biol. Macromol. 160 (2020) 1130–1143.
[72] X. Zhao, Y. Liang, B. Guo, Z. Yin, D. Zhu, Y. Han, Injectable dry cryogels with excellent blood-sucking expansion and blood clotting to cease hemorrhage for lethal deep-wounds, coagulopathy and tissue regeneration, Chem. Eng. J. 403 (2021) 126329.
[73] X. Zhao, B.L. Guo, H. Wu, Y.P. Liang, P.X. Ma, Injectable antibacterial conductive nanocomposite cryogels with rapid shape recovery for noncompressible hemorrhage and wound healing, Nat. Commun. 9 (2018) 1–17.
[74] D. Li, Y. Ye, D. Li, X. Li, C. Mu, Biological properties of dialdehyde carboxymethyl cellulose crosslinked gelatin–PEG composite hydrogel fibers for wound dressings, Carbohydr. Polym. 137 (2016) 508–514.
[75] D. Zhang, Z. Xu, H. Li, C. Fan, C. Cui, T. Wu, M. Xiao, Y. Yang, J. Yang, W. Liu, Fabrication of strong hydrogen-bonding induced coacervate adhesive hydrogels with antibacterial and hemostatic activities, Biomater. Sci. 8 (2020) 1455–1463.
[76] Y. Zhu, J. Zhang, J. Song, J. Yang, T. Xu, C. Pan, L. Zhang, One-step synthesis of an antibacterial and pro-healing wound dressing that can treat wound infections, J. Mater. Chem. B 5 (2017) 8451–8458.
[77] W. Zheng, C. Chen, X. Zhang, X. Wen, Y. Xiao, L. Li, Q. Xu, F. Fu, H. Diao, X. Liu, Layer-by-layer coating of carboxymethyl chitosan-gelatin-alginate on cotton gauze for hemostasis and wound healing, Surf. Coating. Technol. 406 (2021) 126644.
[78] Y. Zhang, M. Chang, F. Bao, M. Xing, E. Wang, Q. Xu, Z. Huan, F. Guo, J. Chang, Multifunctional Zn doped hollow mesoporous silica/polycaprolactone electrospun membranes with enhanced hair follicle regeneration and antibacterial activity for wound healing, Nanoscale 11 (2019) 6315–6333.

[79] Y. Liang, M. Wang, Z. Zhang, G. Ren, Y. Liu, S. Wu, J. Shen, Facile synthesis of ZnO QDs@GO-CS hydrogel for synergetic antibacterial applications and enhanced wound healing, Chem. Eng. J. 378 (2019) 122043.
[80] Y. Song, H. Wu, Y. Gao, J. Li, K. Lin, B. Liu, X. Lei, P. Cheng, S. Zhang, Y. Wang, J. Sun, L. Bi, G. Pei, Zinc silicate/nano-hydroxyapatite/collagen scaffolds promote angiogenesis and bone regeneration via the p38 MAPK pathway in activated monocytes, ACS Appl. Mater. Interfaces 12 (2020) 16058–16075.
[81] J. Hoque, R.G. Prakash, K. Paramanandham, B.R. Shome, J. Haldar, Biocompatible injectable hydrogel with potent wound healing and antibacterial properties, Mol. Pharm. 14 (2017) 1218–1230.
[82] C. Hou, W. He, Z. Wang, B. Yi, Z. Hu, W. Wang, X. Deng, X. Yao, Particulate-aggregated adhesives with exudate-sensitive properties and sustained bacteria disinfection to facilitate wound healing, ACS Appl. Mater. Interfaces 12 (2020) 31090–31098.
[83] M. Li, Z. Zhang, Y. Liang, J. He, B. Guo, Multifunctional tissue-adhesive cryogel wound dressing for rapid nonpressing surface hemorrhage and wound repair, ACS Appl. Mater. Interfaces 12 (2020) 35856–35872.
[84] S. Sharma, R. Kumar, P. Kumari, R.N. Kharwar, A.K. Yadav, S. Saripella, Mechanically magnified chitosan-based hydrogel as tissue adhesive and antimicrobial candidate, Int. J. Biol. Macromol. 125 (2019) 109–115.
[85] L. Huang, Z. Zhu, D. Wu, W. Gan, S. Zhu, W. Li, J. Tian, L. Li, C. Zhou, L. Lu, Antibacterial poly (ethylene glycol) diacrylate/chitosan hydrogels enhance mechanical adhesiveness and promote skin regeneration, Carbohydr. Polym. 225 (2019) 115110.
[86] A. Song, A.A. Rane, K.L. Christman, Antibacterial and cell-adhesive polypeptide and poly(ethylene glycol) hydrogel as a potential scaffold for wound healing, Acta Biomater. 8 (2012) 41–50.
[87] J.-G. Leu, S.-A. Chen, H.-M. Chen, W.-M. Wu, C.-F. Hung, Y.-D. Yao, C.-S. Tu, Y.-J. Liang, The effects of gold nanoparticles in wound healing with antioxidant epigallocatechin gallate and α-lipoic acid, Nanomedicine 8 (2012) 767–775.
[88] Y. Shao, M. Dang, Y. Lin, F. Xue, Evaluation of wound healing activity of plumbagin in diabetic rats, Life Sci. 231 (2019) 116422.
[89] G. Yin, Z. Wang, Z. Wang, X. Wang, Topical application of quercetin improves wound healing in pressure ulcer lesions, Exp. Dermatol. 27 (2018) 779–786.